BioMACROMOLECULES

Article

Reactive oxygen species (ROS)-responsive polymersomes with site-specific chemotherapeutic delivery into tumors via spacer design chemistry

Eliezer Jager, Vladimir Sincari, Lindomar J. C. Albuquerque, Alessandro Jager, Jana Humajova, Jan Kucka, Jan Pankrac, Petr Paral, Tomas Heizer, Olga Janoušková, Rafal Konefal, Ewa Pavlova, Ondrej Sedlacek, Fernando C. Giacomelli, Pavla Pouckova, Ludek Sefc, Petr Stepanek, and Martin Hruby

Biomacromolecules, **Just Accepted Manuscript** • DOI: 10.1021/acs.biomac.9b01748 • Publication Date (Web): 21 Feb 2020

Reactive oxygen species (ROS)-responsive polymersomes with site-specific chemotherapeutic delivery into tumors via spacer design chemistry

Eliézer Jäger,[†,] Vladimir Sincari,[†] Lindomar J.C. Albuquerque,[ϕ] Alessandro Jäger,[†] Jana Humajova,[§] Jan Kucka,[†] Jan Pankrac,[ω] Petr Paral,[ω] Tomas Heizer,[ω] Olga Janouskova,[†] Rafał Konefał,[†] Ewa Pavlova,[†] Ondrej Sedlacek,[†] Fernando C. Giacomelli,[ϕ] Pavla Pouckova,[§] Ludek Sefc,[ω] Petr Stepanek,[†] Martin Hruby[†]*

[†] Institute of Macromolecular Chemistry, Heyrovsky Sq. 2, 162 06 Prague, Czech Republic;

[ϕ] Centro de Ciências Naturais e Humanas, Universidade Federal do ABC, Avenida dos Estados 5001, Santo André, 09210-580, Brazil;

[§] Institute of Biophysics and Informatics, First Faculty of Medicine, Charles University in Prague, Salmovska 1, 120 00 Prague, Czech Republic;

[ω] Center for Advanced Preclinical Imaging (CAPI), First Faculty of Medicine, Charles University, Salmovská 3, Prague 2, 120 00, Czech Republic.120 00 Prague, Czech Republic;

Keywords: chemotherapy, reactive oxygen species, responsive polymers, polymersomes, chemoselectivity; *in vitro*; *in vivo*;

ABSTRACT

The lack of cellular and tissue specificity in conventional chemotherapies along with the generation of a complex tumor microenvironment (TME) limit the dosage of active agents that reaches tumor sites thereby resulting in ineffective responses and side effects. Therefore, the development of selective TME responsive nanomedicines is of due relevance towards successful chemotherapies, albeit challenging. In this framework, we have synthesized novel, ready-to-use ROS-responsive amphiphilic block copolymers (BCs) with two different spacer chemistry designs to connect a hydrophobic boronic ester-based ROS sensor into the polymer backbone. Hydrodynamic flow focusing nanoprecipitation microfluidics (MF) was used in the preparation of well-defined ROS-responsive PSs there were further characterized by a combo of techniques (^{1}H NMR, DLS, SLS, TEM and cryo-TEM). The reaction with hydrogen peroxide releases an amphiphilic phenol or a hydrophilic carboxylic acid which impacts polymersome (PS) stability and cargo release. Therefore, the importance of the spacer chemistry in BCs deprotection and PSs stability and cargo release is herein highlighted. We have also evaluated the impact of spacer chemistry on PS-specific release of the chemotherapeutic drug doxorubicin (DOX) into tumors *in vitro* and *in vivo*. We demonstrate that by spacer chemistry design one can enhance the efficacy of DOX treatments (decrease in tumor growth and prolonged animal survival) in mice bearing EL4 T cell lymphoma. Side effects (weight loss and cardiotoxicity) were also reduced compared to free DOX administration highlighting the potential of the well-defined ROS-responsive PSs as TME selective nanomedicines. The PSs could also find applications in other environments with high ROS-levels, such as, for instance, chronic inflammations, aging, diabetes, cardiovascular diseases and obesity.

INTRODUCTION

The most recent survey by the International Agency for Research on Cancer reported that the global death related to the malignancy was about 9.6 million in 2018 (21% higher than that in 2008).[1,2] This number is predicted to be as high as 19.3 million by 2025[2] calling for improvements in cancer treatments.[3] In this framework, cancer therapies have been tackled to design nanomedicines that can navigate the body and deliver their cargos at desired tumor sites. Nanomedicines able to fast disassemble *in vivo* to release their cargo specifically in TME (including polymer drug-conjugates, polymer micelles and polymersomes (PSs)) are currently investigated as platforms towards more effective tumor treatments.[4-9] Particularly, PSs made from block copolymers (BCs) are spherical self-assembled nanostructures that resemble the cell membranes of living organisms.[10-12] Nevertheless, compared to biological membranes (such as phospholipids), BC vesicles are easier functionalized and their mechanical properties can be finely tuned.[6,7,11] Moreover, enhanced stability and higher loading capacity has been demonstrated as compared to liposomes and micelles.[10-13] These advantages have led to greater interest in recent years towards the development of novel PSs with applications as enzymatic nanoreactors and drug delivery systems, for instance.[6,7,13,14] The PSs are able to encapsulate hydrophobic compounds in the bilayer and hydrophilic drugs in the aqueous lumen,[15,16] and the cargo release can be triggered by external or internal physical or chemical stimuli such as pH, redox potential, light, magnetic field, temperature or the presence of specific enzymes.[13,15,17] The so-called “smart” PSs have been able to release their payloads or show size reduction or charge conversion under the conditions found in tumor microenvironments (reduced pH, hypoxia, tumor-specific enzymes).[15-22] Amongst the aforementioned stimuli, one can explore the presence of higher levels of reactive oxygen species (ROS) in tumour sites.[23,24] ROS, such as hydrogen

peroxide (H_2O_2), are a component of the cellular signaling pathways that are necessary for the growth, development, and fitness of living organisms.[25,26] On the other hand, imbalances in H_2O_2 production lead to oxidative stress and inflammatory events that damage tissue and organs being correlated with the onset and progression of various diseases, including cancer. Hence, the design of PSs able to respond to these inherent features of TME has been proposed as a promising approach for cancer treatments.[19,27]

Taking into account the abovementioned issues, we have developed a novel platform that allows the specific release of bioactive cargo, such as DOX, in response to ROS levels typically found in TME. Well-defined BCs were synthesized by using two different spacer chemistry designs to connect the hydrophobic boronic ester-based ROS sensor to a polymer backbone. The novel materials were further used to prepare oxidative-reductive PSs by using the MF technique. The self-assembled structures were characterized by a variety of techniques and it has been subsequently demonstrated that the employed chemistry plays an important role in BC and PS deprotection rate and on the release of encapsulated double-quenched green bovine serum albumin (DQ-BSA) or DOX. Furthermore, *in vitro* studies suggest that DOX-loaded ROS-responsive PSs could be efficiently delivered into two different tumor cell lines providing enhanced biological activity to the antitumor agent. The *in vivo* biodistribution studies in nude mice bearing EL4 T cell lymphoma demonstrated that the PSs circulate for longer time and they are accumulated to higher extent as compared to the free fluorescent probe. The *in vivo* investigations also highlight that side effects (such as weight loss and cardiotoxicity) were remarkably reduced by using the PSs platforms for DOX release and the effectiveness of the treatment (reduction in tumor growth and prolonged animal survival) can be significantly improved by using specific boronic acid-based monomeric spacers.

EXPERIMENTAL SECTION

Materials

3-Chloro-1-propanol, NaN_3, 3-azido-1-propanol, *N*-ethyl-*N*'-(3-dimethylaminopropyl)carbodiimide hydrochloride (EDC) triethylamine (TEA), hydrogen peroxide (H_2O_2, 30% *w*/*w* solution in H_2O), 4-hydroxymethylphenylboronic acid pinacol ester, 4-aminophenylboronic acid pinacol ester, magnesium sulfate ($MgSO_4$), sodium sulfate (Na_2SO_4), silica gel (70-230 mesh), Sephadex® LH-20, 1-hydroxy-benzetriazol (HOBt), ethanolamine, 4-isopropylphenyl acetic acid, Phorbol 12-myristate 13-acetate (PMA), *N*-acetyl-L-cysteine (NAC) and the chain transfer agent 4-cyano-4-(phenylcarbonothioylthio)pentanoic acid (CTA) were purchased from Sigma-Aldrich and were used as received. Doxorubicin, hydrochloride salt > 99% was purchased from LC Laboratories (USA). Double-quenched green bovine serum albumin (DQ-BSA) was purchased from Thermo Fischer Scientific (Czech Republic). Methanol (MeOH), *N*,*N*-dimethylacetamide (DMAc), diethyl ether (Et_2O), 1,4-dioxane, ethanol, tetrahydrofuran (THF), *N*,*N*-dimethyl formamide (DMF), dichloromethane (DCM), toluene, ethyl acetate, petroleum ether and hexane were purchased from Lachner and dried over molecular sieves (3 Å). Methacryloyl chloride (Sigma-Aldrich) was distilled before use. Deuterated solvents ($CDCL_3$, d_7-DMF, d_6-DMSO, CD_3OD) were purchased from Euriso-top (France). Initiator Azobis isobutyronitril (AIBN, Sigma-Aldrich) was recrystallized from methanol prior to use.

Methods

Synthesis of the azide-containing chain-transfer agent (CTA-Azide). The CTA-Azide was synthetized following the procedure described elsewhere.[28] Briefly, 3-Chloro-1-propanol (3.0 g,

31.7 mmol) and NaN_3 (3.5 g, 54.0 mmol) were dissolved in a mixture of acetone (50 mL) and water (5 mL) in a round bottom flask and refluxed overnight. Acetone was removed under reduced pressure, and 35 mL of water were added to the remaining solution. The product was extracted with diethyl ether (3 × 70 mL), the organic layer was dried over anhydrous Na_2SO_4 and the 3-azido-1-propanol was obtained as a colorless oil (1.6 g, 53%) after solvent removal under reduced pressure. The pure product was analyzed by FTIR. In the step further, a mixture of CTA-COOH (700 mg, 2.51 mmol), 3-azido-1-propanol (380 mg, 3.76 mmol) and dry DCM (40 mL) was added to a round flask equipped with a magnetic bar and a rubber stopper. The solution was cooled to 0 ºC and filled with argon. A solution of EDC (720 mg, 3.76 mmol), DMAP (50 mg, 0.38 mmol) in DCM (10 mL) was added under argon atmosphere to react at 0 ºC for 2 h and then at room temperature overnight. The reaction mixture was washed with water (100 mL, 5 times) and dried over anhydrous Na_2SO_4. The DCM was removed under reduced pressure and the crude product was purified by column chromatography (SiO_2 and hexane/ethyl acetate = 4/1 (v/v)). The pure product (0.38 g, 42%) was characterized by ^{1}H NMR and ^{13}C NMR.

^{1}H NMR (600 MHz, $CDCl_3$, δ): 7.90(d, 2H, Ar H), 7.56 (t, 1H, Ar H), 7.38 (t, 2H, Ar H), 4.26 (t, 2H, CH_2), 3.61 (t, 2H, CH_2), 2.69 (m, 2H, CH_2), 2.60 (m, 1H, CH_2), 2.43 (m, 1H, CH_2), 2.10 (p, 2H, CH_2), 1.93 (s, 3H, CH_3). ^{13}C NMR ($CDCl_3$, δ): 221.49, 171.52, 144.63, 133.22, 129.13, 128.74, 126.81, 118.60, 61.92, 45.85, 41.26, 33.50, 31.52, 29.87, 24.30.

Synthesis of the azide terminated PHPMA macroCTA. *N*-(2-Hydroxypropyl)methacrylamide (HPMA) monomer was prepared as previously described.[28] The synthesis of azide-terminated PHPMA macroCTA was performed by RAFT polymerization. In a Schlenk tube equipped with a magnetic bar, HPMA monomer (1 g, 7 mmol) was dissolved in 6.62 mL of *tert*-butanol. This solution was filled with argon for 15 min and deoxygenated by

three freeze-pump-thaw cycles. The CTA-Azide (118.4 mg, 0.326 mmol) and the initiator AIBN (33.2 mg, 0.204 mmol) were dissolved in 0.736 mL of DMSO and this solution was added to the Schlenk tube and another freeze-pump-thaw cycle was completed. The tube containing the pink solution was filled with argon again and placed into an oil bath at 70 ºC to start the polymerization. After 16 h, the polymerization was quenched by exposing the reaction mixture to air and liquid nitrogen. The polymerization solution was precipitated in a cold mixture of acetone/diethyl ether (*v*/*v* = 3/1) followed by a centrifugation step to isolate the product. The product was dissolved in a small amount of methanol and the azide-terminated PHPMA macroCTA was purified by Sephadex LH-20 using methanol as mobile-phase. The product was precipitated in cold diethyl ether and vacuum dried to yield a pink solid. The obtained polymer was characterized by SEC and ^{1}H NMR (PHPMA mCTA azide M_n = 3 600 g·mol^{-1}, $Đ$ = 1.08).

^{1}H NMR (600 MHz, MeOD, δ): 7.86(s, 2H, Ar H), 7.76 (s, 1H, Ar H), 7.67 (s, 2H, Ar H), 7.45 (bp, 1H, NH), 4.20 (s, 2H, CH_2), 3.88 (s, 1H, CH), 3.41 (s, 2H, CH_2), 3.10 (bp, 2H, CH_2), 2.52 (s, 2H, CH_2), 2.15-1.60 (bp, 2H, CH_2), 1.55-0.90 (bp, 3H, CH_3).

Synthesis of the ROS-responsive monomers 1 and 2. Twenty five millimols (5.48 g) of 4-aminophenylboronic acid pinacol ester (for ROS-responsive monomer 1, M_w = 219.09 g·mol^{-1}) or 4-(hydroxymethyl)phenylboronic acid pinacol ester (5.85 g) (for ROS-responsive monomer 2, M_w = 234.10 g·mol^{-1}) was dissolved in anhydrous DCM (60 mL) followed by the addition of 30 mmol of TEA (3.05 g). After cooling to 0 °C, 30 mmol (3.23 g) of methacryloyl chloride in ~ 5 mL dried DCM was added dropwise within ~ 1 h (temperature not exciding 0 °C). Then, the reaction mixture was warmed to room temperature, stirred for 10 h and filtered. The filtrate was concentrated on a rotary evaporator, diluted by ethyl acetate, and washed with brine thrice. After drying over MgSO4, the organic solution was concentrated and purified by silica column

chromatography using hexane:ethyl acetate (*v*/*v* = 2/1) as eluent. The ROS monomer 1 (M_w = 287.16 g·mol^{-1}) was obtained as a colorless crystal with yield of 80%. The ROS-monomer 2 (M_w = 302.17 g·mol^{-1}) was obtained as a colorless oil with yield of 75%. ROS-monomers 1 and 2 were characterized by ^{1}H NMR.

Nitrogen-containing 4-(*N*-methacryloylaminomethyl)phenylboronic acid pinacol ester monomer - ROS-responsive monomer 1: ^{1}H NMR (600 MHz, $CDCl_3$, δ): 7.76 (d, *J* = 8 Hz, 2H, Ar H), 7.56 (d, *J* = 8 Hz, 2H, Ar H), 7.53 (s, 1H, NH), 5.78 (s, 1H, =CH_2), 5.46 (s, 1H, =CH_2), 2.05 (s, 3H, CH_3), 1.33 (s, 12H, CH_3). ^{13}C NMR ($CDCl_3$, δ): 166.66, 141.11, 140.64, 136.03, 124.93, 120.17, 118.92, 83.95, 25.07, 18.95.

Oxygen-containing 4-(*O*-methacryloylaminomethyl)phenylboronic acid pinacol ester monomer - ROS-responsive monomer 2: ^{1}H NMR (600 MHz, $CDCl_3$, δ): 7.79 (d, *J* = 8 Hz, 2H, Ar H), 7.36 (d, *J* = 8 Hz, 2H, Ar H), 6.14 (s, 1H, =CH_2), 5.57 (s, 1H, =CH_2), 5.19 (s, 2H, CH_2), 1.95 (s, 3H, CH_3), 1.33 (s, 12H, CH_3). ^{13}C NMR ($CDCl_3$, δ): 167.38, 139.32, 136.38, 135.20, 128.94, 127.36, 126.08, 84.05, 25.06, 18.55.

Synthesis of the block copolymers 1 (BC1) and 2 (BC2). In a Schlenk flask equipped with a magnetic bar, PHPMA mCTA azide (100 mg) was dissolved in MeOH (2 mL) and different amounts of ROS-responsive monomer 1 or ROS-responsive monomer 2 (cf. Table 1) and the initiator AIBN (0.5 mol·L^{-1} related to PHPMA mCTA azide) were dissolved in 1,4-dioxane (4 mL) and added to the Schlenk flask under stirring. The solution was filled with argon and three freeze-pump-thaw cycles were performed. Afterwards, the solution was again filled with argon and placed into an oil bath at 70 ºC to start the polymerization. After 24 h, the polymerization was stopped with a quench step using liquid nitrogen. The BCs were obtained after dialysis against deionized water pH 7.4 for 48 h using a dialysis membrane with MWCO 3.5 - 5 kDa.

The water was changed every 12 h and the BCs were recovery by lyophilization. They were further characterized by ^{1}H NMR and SEC.

BC1: $M_n \approx 20.3$ kDa, $Đ = 1.09$; Conversion: 86%; ^{1}H NMR (600 MHz, MeOD, δ): 7.65(bp, 2H, Ar H), 7.40 (bp, 2H, Ar H; 1H, NH), 3.88 (s, 1H, CH), 3.10 (bp, 2H, CH_2), 2.40-1.60 (bp, 2H, CH_2), 1.50-1.25 (bp, 12H, CH_3), 1.25-0.85 (bp, 3H, CH_3).

BC2: $M_n \approx 21.5$ kDa, $Đ = 1.13$; Conversion: 89%; ^{1}H NMR (600 MHz, DMF-d_7, δ): 7.75(s, 2H, Ar H), 7.35 (s, 2H, Ar H; 1H, NH), 4.90 (bp, 2H, CH_2; 1H, OH), 3.85 (s, 1H, CH), 3.05 (bp, 2H, CH_2), 2.15-1.60 (bp, 2H, CH_2), 1.40-1.20 (bp, 12H, CH_3), 1.15-0.80 (bp, 3H, CH_3).

Size exclusion chromatography (SEC). The number-average molecular weight (M_n) and its distribution ($Đ$) were obtained by SEC. SEC of the isolated copolymers was performed at 25 °C with two PLgel MIXED-C columns (300 × 7.5 mm, SDV gel with particle size 5 μm; Polymer Laboratories, USA) and with UV (UVD 305; Watrex, Czech Republic) and RI (RI-101; Shodex, Japan) detectors. DMF was used as a mobile phase at a flow rate of 1 mL·min^{-1}. The molecular weight values were calculated using the Clarity software (DataApex, Czech Republic). Calibration with PMMA standards was used. The M_n and its distribution ($Đ$) for PHPMA macroCTA were determined on a HPLC Shimadzu system equipped with a Superose 12™ column, UV, Optilab rEX differential refractometer and multiangle light scattering DAWN 8 (Wyatt Technology, USA) detectors. These experiment used a 0.3 M sodium acetate buffer/MeOH (pH 6.5, 80:20) containing 0.5 g·L^{-1} sodium azide as the mobile phase.

^{1}H NMR and ^{13}C NMR spectra: ^{1}H NMR spectra of the monomers (300 or 600 MHz) were obtained using a Bruker Avance DPX 300 MHz NMR spectrometer or Bruker 600 MHz NMR spectrometer (for ^{13}C NMR only) with $CDCl_3$ or d_7-DMF as solvents at 25 °C and at 37°C in deuterated PBS/d_7-DMF for polymer deprotection studies (described hereafter). The chemical

shifts are relative to TMS using hexamethyldisiloxane (HMDSO, 0.05 for ^{1}H NMR and 2.0 ppm for ^{13}C NMR) as internal standard. Chemical shifts as, δ, in units of parts per million (ppm).

^{1}H NMR measurements of the polymersomes deprotection. Two milligrams of the BCs were loaded separately into 50 μL of d_7-DMF followed by the addition of 550 μL of deuterated PBS (phosphate buffered saline, pH 7.4). The solution was transferred to a NMR tube and incubated at 37 °C. To the solution, 0.6 μL of H_2O_2 was added to make a 10 mM or 1 mM H_2O_2 solution (H_2O_2 previously diluted). The BCs incubated at 37 °C in deuterated PBS (550 μL) and 50 μL of d_7-DMF were used as control.

Dynamic light scattering (*DLS*). The DLS measurements were performed using an ALV CGE laser goniometer consisting of a 22 mW HeNe linear polarized laser operating at a wavelength λ = 632.8 nm, an ALV 6010 correlator, and a pair of avalanche photodiodes operating in the pseudo cross-correlation mode. The samples were loaded into 10 mm diameter glass cells and maintained at 25 ± 1 °C. The data were collected using the ALV Correlator Control software and the counting time was 30 s. In order to avoid multiple light scattering, the samples were diluted 100 times before the measurements. The intensity correlation functions $g_2(t)$ were analyzed using the algorithm REPES (incorporated in the GENDIST program) resulting in the distributions of relaxation times shown in equal area representation as $\tau A(\tau)$. The mean relaxation time or relaxation frequency ($\Gamma = \tau^{-1}$) is related to the diffusion coefficient (D) of the nanoparticles as $D = \Gamma/q^2$ where $q = (4\pi n sin(\theta/2))/\lambda$ is the scattering vector being n the refractive index of the solvent and θ the scattering angle. The hydrodynamic radius (R_H) or the distributions of R_H were calculated by using the well-known Stokes-Einstein relation:

$$R_H = (K_B T)/6\pi n D \qquad \text{equation 1.}$$

being k_B the Boltzmann constant, T the absolute temperature and η the viscosity of the solvent.

Static light scattering (*SLS*). In the SLS mode, the scattering angle was varied from 30 to 150° with a 10° stepwise increase. The absolute light scattering is related to weight-average molar mass ($M_{w(\mathrm{PSs})}$) and to the radius of gyration (R_{G}) of the nanoparticles by the Zimm formalism represented as:

$$Kc/R_\theta = 1/M_w\,(1 + R_G^2 q^2/3) \qquad \text{equation 2.}$$

where K is the optical constant which includes the square of the refractive index increment (dn/dc), R_θ is the excess normalized scattered intensity (toluene was used as standard solvent) and c is the polymer concentration given in mg·mL^{-1}. The refractive index increment (dn/dc) of the PSs in pure water was determined using a Brice-Phoenix differential refractometer operating at λ = 632.8 nm. (respectively 0.180 mL/g and 0.173 mL/g for PS1 and PS2).

Electrophoretic light scattering (*ELS*). The ELS measurements were employed in order to determine the average zeta potential (ζ) of the PSs, which has been performed using a Zetasizer NanoZS instrument (Malvern Instruments, UK). The equipment measures the electrophoretic mobility (U_{E}) and converts the value to ζ-potential (mV) through the Henry's equation. The Henry's function was calculated through the Smoluchowski approximation.

Transmission electron microscopy (*TEM*) *and cryogenic transmission electron microscopy* (*cryo-TEM*). TEM observations were performed on a Tecnai G2 Spirit Twin 120kV (FEI, Czech Republic) using a bright field imaging mode at accelerating voltage 120 kV. The nanoparticles (4 µL) were dropped onto a copper TEM grid (300 mesh) which was coated with thin, electron-transparent carbon film. The excess of the solution was removed out by touching the bottom of the grid with filtering paper. This fast removal of the solution was performed after 5 min of sedimentation in order to minimize oversaturation during the drying process. Afterwards, the samples were negatively stained with uranyl acetate (2 µL of 1 wt. % solution

dropped onto the dried polymersomes and removed after 30 s as described above). The samples were left to dry at room temperature and then observed in the TEM microscope. Under these conditions, the micrographs displayed negatively stained background with bright polymersomes. The image analysis was performed using the Image J software. The polymersomes were also imaged by Cryo-TEM where 4 μL of the sample solution were loaded into an electron microscopy grid covered with a holey or lacey carbon supporting film (Electron Microscopy Science) which was hydrophilized just before the experiment via glow discharge (Expanded Plasma Cleaner, Harrick Plasma, USA). The excess of the solution was removed by blotting (Whatman no. 1 filter paper) for ~ 1 s, and the grid was plunged into liquid ethane held at -182 °C. The vitrified sample was then immediately transferred into the microscope and observed at -173 °C at the accelerating voltage of 120 kV.

Polymersomes production by microfluidics. The PSs were produced after testing different polymer concentrations, organic solvents and flow-rates of the organic and aqueous phases according the method previously described.[28] Briefly, BC1 and BC2 were dissolved in THF/MeOH (80/20) (*v*/*v*) to produce a final concentration of 5.0 mg·mL^{-1}. Polymersomes were produced using the microfluidic device setup from Dolomite (Royston, United Kingdom) equipped with a glass Micromixer chip with 12 mixing stages micro-channels of 50 μm × 125 μm (depth x width). The polymer solution was pumping through the middle channel and PBS through the side channels using two independent Dolomite Mitos P-Pump (Royston, United Kingdom) controlled *via* PC software. For the production of DOX-loaded PS, the drug (1 mg·mL^{-1}) was dissolved in PBS. All solutions were previously filtrated (0.22 μm). The flow rates were 200 μL·mL^{-1} for water phase and 100 μL·mL^{-1} for organic phase, resulting in flow rate ratio 2:1. The polymer colloids were collected in vials and dialysed against PBS for 12 h to remove

the organic solvent and unloaded DOX. They were further characterized by DLS, SLS, ELS and TEM. DOX was determined by UV-Vis using an analytical curve with linear response in the range 0.001 - 0.5 mg·mL^{-1}. DOX loading content (LC) and DOX loading efficiency (LE) were calculated using the standard equations:

$$LC\ (\%) = (\text{DOX ammount in PSs})/(Mass\ of\ PSs)\ x\ 100 \qquad \text{equation 3.}$$

$$LE\ (\%) = (\text{DOX ammount in PSs})/(\text{DOX feeding})\ x\ 100 \qquad \text{equation 4.}$$

The quantifications were always performed in triplicate and the mean values are reported throughout the manuscript.

The Cy7-PS1 and Cy7-PS2 conjugates containing the Cy7 fluorescent dye were also produced by microfluidics. Firstly, the coupling between the fluorescent dye Cyanine 7-DBCO (Cy7) and the azide terminated BC1 and BC2 was performed by using an adapted procedure as described elsewhere.[28] Briefly, in an amber glass vial, 30 mg of the BCs were dissolved in 1 mL of DMF under stirring. The fluorescent dye (Cyanine 7-DBCO) was added in the molarity 5:1 (fluorescent dye:azide terminated group) and keep reacting overnight in the dark. Afterwards, the solution was dialyzed in a float lyzer 3.5-5 kDa against water for 24 h to remove free dye and organic solvent. The Cy7-BC1 and Cy7-BC2 conjugates were recovery by lyophilization with yield ~ 60 %. For the production of the Cy7-PSs, the BCs powder were mixed 1:1 weight ratio (BC1:Cy7-BC1 and BC2:Cy7-BC2) and the mixtures were dissolved in THF/MeOH (80/20 *v/v*) to produce final concentrations of 5.0 mg·mL^{-1}. The chemical structure of the Cy7-BC2 conjugate is shown in Supporting Information. The PSs were produced as mentioned before and the amount of Cy7 fluorescent dye was measured by fluorescence spectroscopy (750 nm Ex / 780 nm Em) and adjusted to 30 μg·mL^{-1} for both PSs.

In Vitro Drug Release: The *in vitro* DOX release was investigated in PBS and PBS with 1 mM H_2O_2 at 37 °C by using the dialysis method. A pre-swollen cellulose dialysis membrane tube with MWCO 3.5-5 kDa (Spectra-Por® Float-A-Lyzer® G2) was filled with 2.0 mL of DOX-loaded-PSs at 0.5 mg·mL^{-1}. The membrane tube was then immerged into 3 L of PBS at 37 °C and 350 rpm. At pre-determined times, 10 µL of the DOX-loaded PSs was removed and diluted into 90 µL of MeOH for the determination of the remaining DOX. The DOX amount was quantified by UV-Vis at λ = 480 nm.

Cell Culture: The T-lymphocyte derived human cell line Jurkat (LGC standard, Poland) was cultured in RPMI-1640 medium supplemented with 100 units of penicillin and 100 µg·mL^{-1} streptomycin (Thermo Fischer Scientific, Czech Republic) with fetal bovine serum. The T-lymphocyte murine cell line EL4 (LGC standard, Poland) was cultured in Dulbecco's Modified Eagle's Medium (DMEM) supplemented with 100 units of penicillin and 100 µg·mL^{-1} streptomycin (Thermo Fischer Scientific, Czech Republic). Both cell cultures were incubated and cultivated in a humidified incubator at 37 °C with 5% CO_2 in 25 cm^2 flasks.

Cellular Uptake: Both cell lines were plated into 24-well plate at density 1 × 10^5 cells per well the day before incubation with PSs. PSs were incubated with cells for 2 h in 5% CO_2 at 37 °C. The amount of DOX-loaded PSs was normalized to DOX content (10 µg·mL^{-1}). After the incubation time, the cells were centrifuged (1500 rpm) and washed two times with 0.5 mL PBS containing 0.5% BSA. The cells were then resuspended in PBS/BSA and analyzed by flow cytometry using a FACS Verse (Becton Dickinson) (1 × 10^4 events per sample) apparatus. The data were processed using the FlowJo software V7.6.1. The median of the fluorescence intensity were determined and the signal of negative cells was subtracted to

calculate the relative uptake (Dox median of fluorescence was assigned as 100%). Untreated cells and cells incubated with DOX only were used as the controls. All samples were measured in duplicate in four independent experiments.

Cell Viability Assays: Cell viability assays were conducted using the Alamar Blue® cell viability reagent (Thermo Fischer Scientific, Czech Republic) according to the manufacturer`s protocol. Cells were seeded in 100 μL of media into 96-well plates 24 h prior to treatment at a density of 1×10^4 cells per well. Serial dilutions of PSs and DOX were added to the medium (10 μL). The cells were subsequently incubated for 72 h in 5% CO_2 at 37 °C. After the incubation time, 10 μL of Alamar Blue® reagent was added to each well and incubated for 4 h in 5% CO_2 at 37 °C. Resorufin that is reduced from resazurin is the active compound of Alamar Blue® reagent. Resorufin is highly fluorescent only in viable cells and its intensity was measured by using a Synergy Neo plate reader (Bio-Tek, Prague, Czech Republic) at 570 nm $_{Ex}$ / 600 nm $_{Em}$. DOX-free PSs (concentrations from 0.1625 μg up to 100 $\mu g \cdot mL^{-1}$), untreated cells and cells incubated with free DOX were used as the controls. All samples were measured in triplicate in three independent experiments.

DQ-BSA Assay: In order to determine the intracellular degradation of the polymersomes, EL4 cells were plated into 96-well plate at density 3×10^4 cells per well the day before incubation with PSs. DQ-BSA-loaded PSs (1 $mg \cdot mL^{-1}$; DQ-BSA adjusted to 50 $\mu g \cdot mL^{-1}$ by UV-Vis) were incubated with cells for 2 h in 5% CO_2 at 37 °C. For PMA-treated cells, PMA was added (100 nM) 1 h after the 2 h incubation time (aforementioned). For NAC-treated cells, NAC was added (3 mM) at the same time of the DQ-BSA-loaded PSs and 1 h after PMA (100 nM) was added. After the incubation time, the cells were resuspended with 0.5 mL PBS containing 0.5% BSA and analyzed by flow cytometry using a BD FACS

Aria II (Becton Dickinson, USA) (1×10^4 events per sample). The data were processed using the FlowJo software V7.6.1. The median of the fluorescence intensity was determined and the signals of negative cells were subtracted for calculation of DQ-BSA intracellular degradation. All samples were measured in duplicate.

In vivo biological studies: The animal experiments described in this study were performed in accordance with the corresponding legislation in the Act on Experimental Work with Animals (act no. 246/1992 of the Czech Republic and decrees no. 419/2012) which is fully compatible with the corresponding European Union directives. For the antitumor effect of the PSs, it has been used healthy inbred C57BL/6J mice (females, 8 weeks old, obtained from AnLab, Ltd., Prague, Czech Republic). After the mice were shaved, EL4 lymphoma carcinoma cells (1×10^5 cells in PBS) were injected subcutaneously into the right flank. When the tumors reached the diameter of 4-5 mm, the animals were randomly divided into 4 groups (n = 8). Subsequently, the first group received PBS (named saline group) intravenously into the tail vein. Injection was repeated on days 4 and 8 from the first application (day 0). The second group received the DOX-free formulation (5 mg DOX (equivalent)/kg dissolved in PBS in the same days as well as DOX-loaded PS1 and PS2 formulations (100 μg DOX in 5 mg of PSs in 250 μL). Subsequently, the survival of all animals was monitored for 40 days and tumor volume was measured twice a week using the equation 5 where *a* is the length and *b* is the width of the tumor.

$$V = (a \times b^2 \times \pi)/6 \qquad \text{equation 5.}$$

Biodistribution studies: Biodistribution of Cy7-PS1, Cy7-PS2 and free Cy7 was determined by fluorescence intensity in athymic nude mice 0, 4, 8, 24, 48, 96 and 144 h after intravenous injection (mice injected with 250 μL of PSs containing 30 μg Cy7/mL; PSs ~ 10 mg). Fluorescence was detected by using the Xtreme *In Vivo* Imaging System (Bruker, Germany). For

fluorescence imaging, the excitation filter 750 nm and emission filter 830 nm were used. During the measurements, mice were anesthetized using 2 % isoflurane (Aerrane, Baxter, UK). The greyscale adjustments and quantification of the fluorescence intensity were performed using open source image processing software Fiji. Regions of interest (ROI) were selected based on tumor boundaries visible in reflectance and the mean fluorescence intensity in the tumors was calculated as fluorescence intensity in ROI divided by area of ROI. Mice were sacrificed 144 h after administration of polymersomes and the fluorescence intensity was measured in tumor, heart, intestine, kidneys, liver, lungs and spleen. The signals were normalized by the weight of the organs.

Peripheral blood collection: Peripheral blood was collected with capillaries containing ~ 2 μL of 0.5 mol·L^{-1} ethylenediaminetetraacetate (EDTA) solution (Sigma Aldrich, Czech Republic) from the retro orbital sinus of anaesthetized animals (using inhalation anesthesia with 3% isoflurane). The first blood samples were taken before EL4 cells application and the subsequent blood samples in the following 7 day intervals. The blood samples were analyzed with a BV5300 veterinary haemoanalyzer (Mindray, China) and by using flow cytometry.

Determination of creatine kinase levels: Blood samples were collected from the retro orbital plexus under inhalation anesthesia using 3 % isoflurane, into non-heparinized capillary tubes at the day 10 after the third injection of free DOX, PS1, PS2 and saline groups. Plasma was separated by centrifugation at 4000 rpm and 4 ºC and further stored at -80 ºC until analysis. Creatine phosphokinase enzyme activity levels were quantified using a commercially available kit, Creatine Kinase Activity Assay Kit (Sigma Aldrich, Czech Republic) based on the protocol described by the manufacturer.

Statistical Analysis: The two-way ANOVA test has been applied to identify statistical differences among groups. Survival curves were generated using the Kaplan-Meier method. Analyses were performed with GraphPad Prims 6 software (GraphPad Inc, United States) and $P < 0.05$ was considered statistically significant.

RESULTS AND DISCUSSION

Synthesis of the ROS-responsive building blocks. The ROS-responsive BCs backbones were envisaged based on pinacol-type boronic ester protecting groups (Figure 1a, green and 1b, red and Figure S1). Amongst the oxidative-responsive moieties, boronic acids and boronic esters undergo oxidation-triggered hydrolysis in the presence of biologically relevant levels of H_2O_2 thereby making these compounds candidates for ROS-induced polymer decomposition. The pinacol-type boronic ester groups have been shown to be the most ROS-selective and sensitive probes to respond to H_2O_2 at physiological concentrations with high specificity.[29-32] At physiologically relevant H_2O_2 concentrations (100 μM - 1 mM of H_2O_2),[31,33,34] benzylic based boronic esters are oxidized to phenols, which will then undergo a quinone methide rearrangement leading to a strong hydrophilization of the polymer block (discussed hereafter) and subsequent PSs disassembly and cargo release (Figure 1c).

Accordingly, under the envisaged targeted site-specific ROS-rich environment, derivative benzylic ester can undergo complete self-immolative deprotection resulting in a hydrophilic polymer after reaction, while partial deprotection occurs in the aniline derivative, resulting in a relatively less hydrophilic polymer containing phenols (Figure 1a and 1b). The polymer poly([*N*-(2-hydroxypropyl)]methacrylamide) (PHPMA) (Figure 1a, blue) has been chosen as the hydrophilic segment due to its stealth property and biocompatibility. The polymer block PHPMA

bearing azide functional groups was synthesized using the HPMA monomer and a modified chain transfer agent (CTA) by the reversible addition-fragmentation chain transfer (RAFT) polymerization and it was used as a macro chain transfer agent (PHPMA mCTA azide, M_n = 3.6 kDa, $Đ$ = 1.08; Figure S1a, Figure S2 and Table 1). The introduction of the clickable azide group to the end of the PHPMA BCs allows further PSs functionalization with fluorescent dyes or antibodies for imaging and selective targeting, for instance. Subsequently, the 4-aminophenyl boronic acid pinacol ester (compound 1, Figure S3) was reacted with methacryloyl chloride to generate the methacrylamide pinacol ester-protected ROS monomer 1 (Figure S1b and Figure S3). 4-(hydroxymethyl)phenylboronic acid pinacol ester (compound 2, Figure S3) was methacryloylated to generate the methacrylate pinacol ester-protected ROS monomer 2 (Figure S1c and Figure S3). The ROS methacrylic monomers were further polymerized using the PHPMA mCTA azide to generate the ROS-responsive amphiphilic BC1 (Figure 1a, Figure S1b) and ROS-responsive amphiphilic BC2 (Figure 1b, Figure S1c). The BCs were successfully synthetized by RAFT polymerization with similar M_w and desired polydispersity (Table 1).

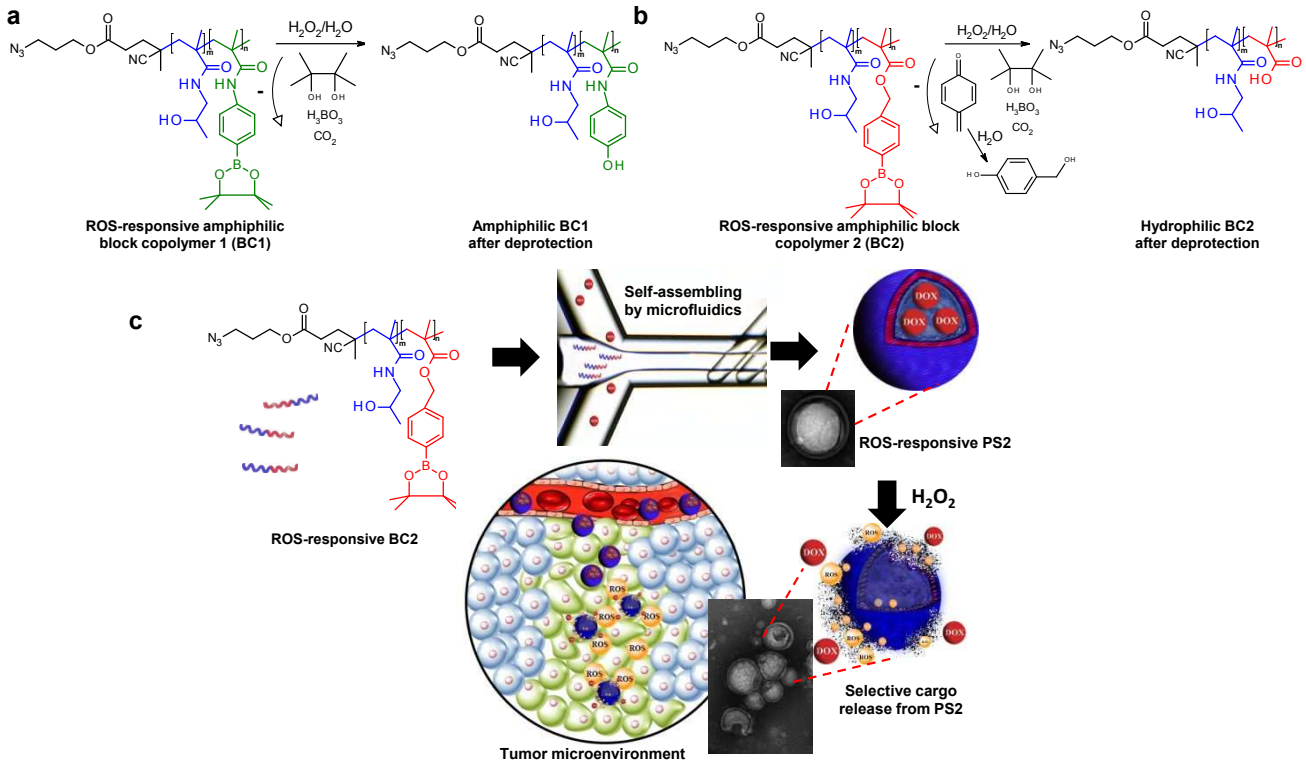

Figure 1 Spacer design chemistry envisaged BC1 (a) and BC2 (b) and their respective mechanism of ROS-triggered deprotection by H_2O_2. PHPMA in blue, nitrogen-containing boronic spacer ("amphiphilic" - partially hydrophilic, BC1) in green and oxygen-containing boronic spacer (fully hydrophilic, BC2) in red. c) Microfluidics manufacturing of DOX-loaded PS2 from BC2 and the ROS deprotection under H_2O_2. Cargo chemotherapeutic DOX release is shown in red.

We targeted the synthesis of BCs with the appropriate hydrophilic:hydrophobic weight ratio (ϕ = weight fraction of the hydrophilic block at the BCs 10 ~ 40 %)[16,28] (Table 1) aiming the preparation of PSs enabling the DOX solubilisation in their aqueous lumen. Successful BC synthesis was confirmed by ^{1}H NMR (Figure S4) and size exclusion chromatography (SEC) analysis (Figure S5). The M_n of BC1 is ~ 20.3 kDa with low dispersity $Đ$ ~ 1.09 and these values

are M_n ~ 21.5 kDa and $Đ$ ~ 1.13 for BC2 as determined by SEC (Table 1 and Figure S5). The characteristic proton signals corresponding to the repeating units of the monomers are assigned in the ^{1}H NMR spectra given in Figure S4.

Deprotection of the ROS-responsive building blocks

The deprotection of the BCs was followed by ^{1}H NMR at 1 mM and 10 mM H_2O_2 environments in d_7-DMF/PBS pH 7.4.[31,33,34] The Figure 2 shows high-resolution ^{1}H NMR spectra of BCs recorded from 5 min to 24 h after the addition of 1 mM or 10 mM H_2O_2. The spectra portrayed in Figure 2a-b (5 min, bottom) evidence weak and broad signals from the hydrophobic block and strong signals from the hydrophilic PHPMA block for both BC1 (Figure 2a) and BC2 (Figure 2b) prior to H_2O_2 addition. These results demonstrate that the protons corresponding to the hydrophobic block are restricted in mobility (not observed in spectra), whereas the protons of the PHPMA block corresponding to the hydrophilic segment of the BCs are visible. Nevertheless, different behaviours after H_2O_2 addition were observed for BC1 (Figure 2a, top) and BC2 (Figure 2b, top). The aryl boronic ester groups of BC1 are oxidized and subsequently hydrolysed evidencing the stable intermediate 4-amino-phenol that does not undergo quinone methide rearrangement. On the other hand, for BC2, the aryl boronic ester groups are oxidized and hydrolysed with the intermediate phenol in water quickly turning to 4-(hydroxymethyl)phenol (Figure 1b and Figure 2b). The ^{1}H NMR spectra evidence that the side chains of the BCs are fully deprotected after 24 h (BC1, Figure 2a and Figure S6; BC2, Figure 2b and Figure S7) in 10 mM H_2O_2 environment. The deprotection is time- and H_2O_2 concentration-dependent as evidenced by the course of the pinacol alcohol appearance (Figure 2c), product of deprotection of the pinacol ester protected boronic groups. For BC2 (Figure 2b, top) it is clearly

observed that the broad peaks in the ^{1}H NMR spectrum related to the BC are replaced by the sharp peaks of the low molecular weight side groups, demonstrating subsequent self-immolative reaction triggered by H_2O_2. The self-immolative reaction proceeds more extensively by increasing incubation time or H_2O_2 concentration as observed by evaluating the time dependence ^{1}H NMR integral intensities of the appearance of 4-(hydroxymethyl)phenol group (Figure 2d). The former group is a product of the quinone methide rearrangement on the benzylic group that takes place only in BC2 (Figure 1b, Figure 2d, Figure S6 and S7). This step of deprotection is slower and after 60 h (in 10 mM H_2O_2) ~ 53 % of BC2 underwent self-immolative reaction (Figure 2d, black squares and Figure S7b). Comparison between the spectra were also recorded in solvents suitable for both blocks (MeOD, d_7-DMF, cf. Supporting Information, Figure S4).

We further evaluated the H_2O_2 scavenging ability of the BCs. In the experiment, 1 mg of BC1 and BC2 were added to 1 mL of different H_2O_2 concentrations (200 and 100 μM) and after 3 h of incubation, the concentration of H_2O_2 in the supernatants was determined by the Amplex Red Hydrogen Peroxide/Peroxidase Assay.[35] The Figure S8 evidences that both BCs are reactive to H_2O_2 at similar extents (poly(lactic) acid-*block*-poly(ethylene) oxide (PLA-*b*-PEO) was used as a control). The similar ability of both BCs to react with H_2O_2 is probably due to the similar amounts of pinacol-protected boronic groups (Table 1). We highlight that both BCs respond to pathophysiological relevant levels of H_2O_2 ($\lesssim$ 1 mM).[26,33]

Table 1. Synthetic parameters and molecular weight data of the polymers prepared *via* RAFT polymerization.

(Co)polymer code	Sample	$[M]_0/[CTA]_0/[I]_0$	Time (h)	Conversion (%)[a]	$M_{n,\,th}$[b] (g·mol)$^{-1}$	$M_{n,\,SEC}$ (g·mol)$^{-1}$	$M_{n,\,NMR}$ (g·mol)$^{-1}$	$Đ$	ϕ^h (%)
P(HPMA)	$P(HPMA)_{37}$	100/2/1[e]	16h	46	7200	3600[c]	5300	1.08[c]	-
BC1	$P[(HPMA)_{37}$-*b*-$(ROS\text{-}1)_{31}]$	100/2/1[f]	24h	86	30200	20300[d]	14200	1.09[d]	18
BC2	$P[(HPMA)_{37}$-*b*-$(ROS\text{-}2)_{42}]$	100/2/1[f]	24h	89	28700	21500[d]	18000	1.13[d]	17

[a] Determined by ^1H NMR in D_2O; [b] Theoretical $M_n = [M]_0/[CTA]_0 \times$ conversion $\times M_{w(monomer)} + MW_{CTA}$; [c] Determined by SEC in MeOH/acetate buffer pH 6.5, 80/20 vol. %; [d] Determined by SEC in DMF using PMMA as standard; [e] conditions: tert-butanol, $[M]_0$ = 1.5 M, 70 °C; [f] conditions: 1,4-dioxane/MeOH, 60/40 vol. %, $[M]_0$ = 3 M, 70 °C; [g] Weight fraction of the hydrophilic block (SEC).

Characterization of the ROS-responsive polymersomes

Block copolymers containing hydrophilic PHPMA and hydrophobic boronic-based monomer in a given weight ratio and with desired molecular weight can generate self-assembled PSs in aqueous solution.[10,16,28] The manufacturing of the self-assemblies has been conducted by using the microfluidic technique.[28] Spherical and uniform PSs were obtained from both BCs after dialysis and they were detailed characterized by dynamic (DLS), static (SLS) and electrophoretic (ELS) light scattering, transmission electron microscopy (TEM) and cryogenic TEM (cryo-TEM). The size distribution are monomodal with average diameter $D_H \sim 120$ nm (PDI = 0.09) for PS1 (Figure 2e, black circles) and $D_H \sim 132$ nm (PDI = 0.10) for PS2 (Figure 2e, blue circles) after 24 h in PBS. The DOX loading leads to a gentle increase in the diameter (~ 5-10 nm) and polydispersity (~ 0.18) of PS2 (Table 2) although not affecting their stability and applicability.

Table 2. Structural features of the manufactured PSs as determined by light scattering measurements.

PSs	R_H (nm)[a] Diameter = $2R_H$	PDI[a]	ζ[b] (mV)	R_G[c] (nm)	$\rho^c = R_G/R_H$	M_W[c] PS $\times 10^7$ (g·mol^{-1})	N_{Agg}[c/d]
PS1	60.0	0.09	- 8.4	65	1.1	5.45	2460
PS2	65.0	0.10	-8.9	64	1.0	6.06	2450
DOX-PS1	62.5	0.15	-8.5	-	-	-	-
DOX-PS2	68.0	0.18	-8.2	-	-	-	-
PS1,10 mM H_2O_2	63.0	0.10	-15.4	50	0.8	5.29	2388
PS2,10 mM H_2O_2	62.0	0.08	-23.4	56	0.9	3.12	1280

[a)]Dynamic light scattering; [b)] Electrophoretic light scattering; [c)] Static light scattering; [d)]Weight-average molecular weight (M_w) of the BC;

The combination of DLS and SLS data (Figure S9) provides important information regarding the structural features of the assemblies. The ratio $R_G/R_H \sim 1.0$ (Table 2) is characteristic of hollow spheres (vesicles).[28,36] The high numbers for N_{Agg} are also expected for the vesicular morphology.[28,37] The size and morphology were confirmed by TEM images portrayed in Figure 2f (PS2) and Figure S10a (PS1) where spherical and homogeneous PSs are observed.

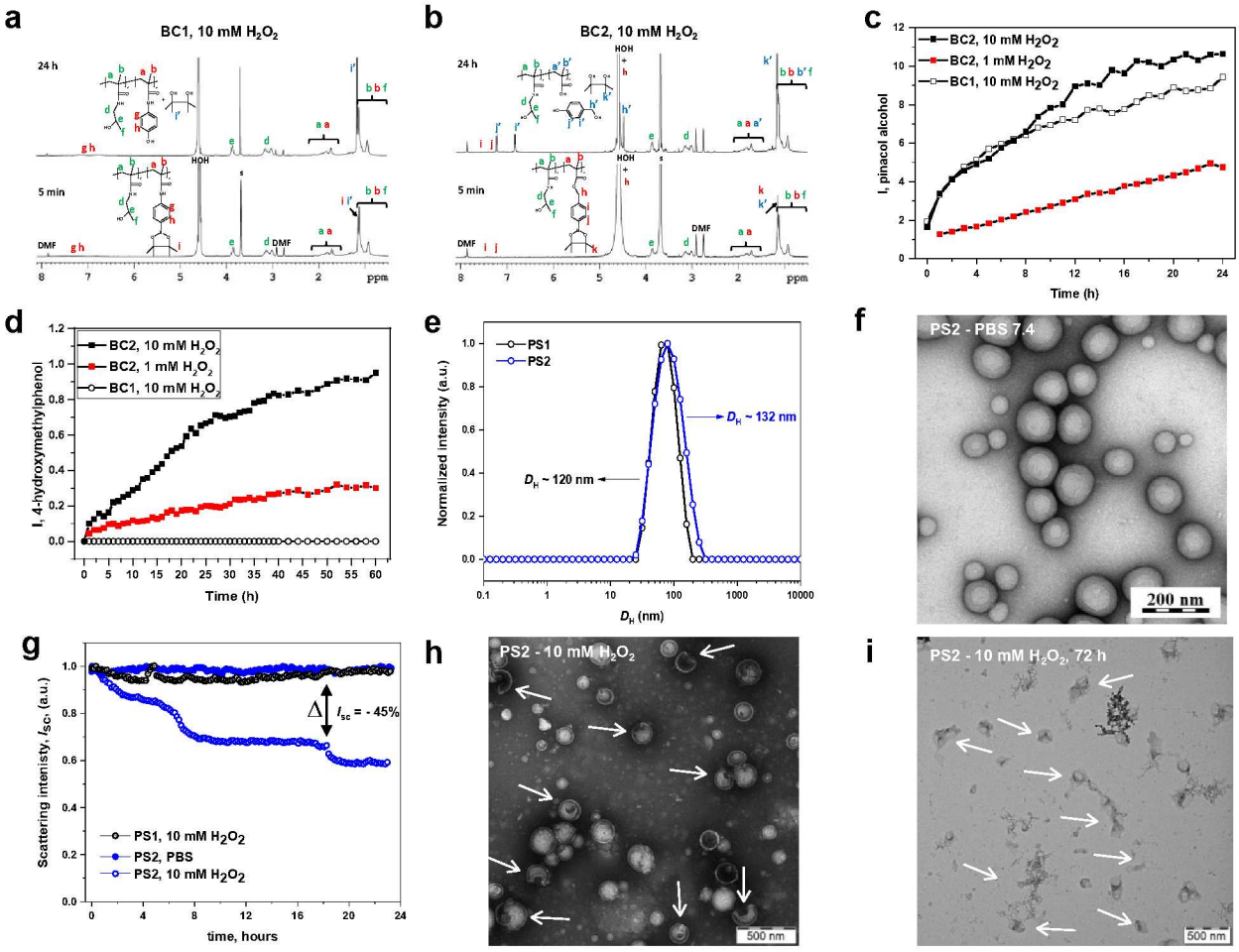

Figure 2 a) ^{1}H NMR spectra of BC1 (a) and BC2 (b) deprotection after 5 min (bottom) and 24 h (top) of incubation in 10 mM H_2O_2 in d_7-DMF, deuterium PBS. (c) ^{1}H NMR integral intensities related to the deprotection of the pinacol ester protected boronic groups and appearance of pinacol alcohol, product of the degradation, along 24 h of incubation of BC1 in H_2O_2 10 mM (open black circles) and BC2 in H_2O_2 1 mM (solid red squares) or 10 mM (solid black squares). (d) ^{1}H NMR integral intensities related to the appearance of 4-hydroxymethyl phenol, product of degradation of BC2, during 60 h of incubation in H_2O_2 1 mM (solid red squares) or 10 mM (solid black squares) and BC1 during 60 h of incubation in H_2O_2 10 mM (open black circles). (e) Distributions of diameters for PS1 (open black circles) and PS2 (open blue circles) in PBS pH

7.4 and TEM micrographs of PS2 upon incubation in PBS pH 7.4 (f). Changes in light scattering intensity (I_{sc}) after incubation of PS2 in PBS pH 7.4 (solid blue circles) and 10 mM H_2O_2 (open blue circles) and PS1 (open black circles) at 37 °C during 24 h (g). TEM micrographs of PS2 after 24 h (h) and 72 h (i) of incubation in 10 mM H_2O_2 (arrows depict the deprotected or disassembled PS2).

Subsequently, the PSs stability was evaluated under relevant H_2O_2 concentration (10 mM H_2O_2) as a function of time to demonstrate the ROS responsiveness.[31,33,34,38] The PSs are stable without changes in particle size during 24 h of incubation in PBS at pH 7.4 (Figure 2e); Nevertheless, polymer deprotection and particle damage is observed after incubation with H_2O_2. For PS2, the scattering intensity (I_{sc}) drops almost 2-fold (Figure 2g, blue open circles) compared with I_{sc} in PBS (Figure 2g, blue filled circles) and PS1 in 10 mM H_2O_2 (Figure 2g, open black circles). The more negative surface charge (ζ-potential) after H_2O_2 incubation also suggests the deprotection of PS2 to the final carboxyl groups (Figure 1b and Table 2). The DLS data agree with ^{1}H NMR deprotection experiments discussed above and confirms that the deprotection (followed self-immolative reaction) of BC2 is more evident than in BC1 (Figure 2 and Figure S6 and S7). For BC2, H_2O_2-triggered polymer deprotection is most likely due to the surface-eroded PSs (decrease in I_{sc} ~ 45 %) (Figure 2g). The changes in I_{sc} is mostly related to the reduction in $M_{w(PS2)}$ (Table 2, Figure S9) although thinly change in the refractive index of the polymer has been monitored (from 0.173 mL·g^{-1} to 0.166 mL·g^{-1} before and after deprotection, respectively).

The PS2 has been also imaged by TEM after incubation in 10 mM H_2O_2 (Figure 2h-i). The PS2 self-assemblies become irregular after 24 h incubation (Figure 2h, arrows) and vanish after 72 h (Figure 2i). The polymeric vesicles were complementary imaged by cryo-TEM (Figure

S10b and S10c) and surprisingly, PS2 showed little difference in morphology after incubation in H_2O_2 (Figure S10c), in contrast with PS2 incubated in PBS for 72 h (Figure S10b), suggesting that they are still not completely damaged. Nevertheless, they are much more permeable after H_2O_2 incubation in agreement with the reduction in light scattering monitored (Figure 2g, open blue circles). The contrast change upon incubation in H_2O_2 is confirmed by plotting the profile of the gray value of the particles using the Image J software (Figure S10 b-c, inset).

In vitro assays

The ROS-responsiveness of the manufactured polymersomes evidenced by ^{1}H NMR, DLS, TEM and cryo-TEM was expected to influence the release of DOX encapsulated into their aqueous lumen. To evaluate this feature, DOX-loaded PSs have been prepared. The values of LE and LC were determined by UV-Vis (LE = 36.5 % and LC = 3.65 % for DOX-PS1 and LE = 34.2 % and LC = 34.2 % for DOX-PS2). The DOX release was monitored *in vitro* by UV-Vis during 24 h of incubation in PBS or 1 mM H_2O_2. DOX release in the H_2O_2 environment is faster than in PBS regardless the polymersome, although faster release is monitored for PS2 (Figure 3a). Both PSs released DOX twice faster in the simulated ROS-rich microenvironment compared to the release in PBS. This behaviour preliminary suggests that it could play an important role in the cytotoxicity to cancer cells.[32-34] In the step further, we evaluated the cellular uptake of DOX-loaded PSs in EL4 and Jurkat lymphoma cells. The cell lines were selected due to their clinical relevance (DOX is frequently used in the treatment of lymphoma tumours) and due to their ROS overproduction.[39-40] The presence of DOX (470 nm $_{Ex}$ / 585 nm $_{Em}$) enable the investigation of cellular uptake by flow cytometry. Free DOX, and PS1 and the PS2 with DOX-loaded equivalent amounts were incubated with the cells and fluorescent intensity has been monitored. The results

provided in Figure 3b evidence similar uptakes of PS1 and PS2 regardless the cell line. Indeed, the cellular uptake of nanostructures is influenced by particle size, shape and surface charge, for instance. Nevertheless, the similar uptake behaviour is probably due to the identical chemical nature of the nanoparticle´s shell (PHPMA-stabilized assemblies). Additionally, both assemblies are spherical with similar size and surface charge (Table 1).

Afterwards, the *in vitro* therapeutic effect of DOX-loaded PSs for Jurkat and EL4 cells was evaluated by using the alamarBlue® assay after 72 h incubation time. Drug-free PSs were also evaluated up to the maximum concentration of 100 $\mu g \cdot mL^{-1}$. In such cases, the cell viability was never smaller than ~ 60% (Figure S12). The cytotoxicity of free DOX and DOX-loaded PSs is similar as confirmed by the IC_{50} values (Figure 3c and 3d). The slightly lower IC_{50} value for free DOX, particularly to EL4 cells, is probably due to its ability to diffuse into the cell nuclei.[42-44] Nevertheless, the cytotoxicity of free DOX and DOX-loaded PSs is similar at higher DOX concentrations, pointing out the effectiveness of both formulations against the cancer cell lines. Accordingly, although free DOX is uptaken to higher extent (Figure 3b), the biological activity is similar to that of DOX-loaded PSs suggesting that the ROS-responsiveness helps the intracellular delivery of the active agent endorsing an efficient cytotoxic effect. Indeed, in order to demonstrate nanoparticle´s intracellular degradation, PSs were also loaded with double-quenched DQ-BSA that emits fluorescence upon protease cleavage.[45] They were further incubated with EL4 cells, and the fluorescence intensity was monitored by flow cytometry (Figure 2e). The cells were also treated with the ROS inducer phorbol 12-myristate 13-acetate (PMA, 100 nM).[46] In the presence of PMA, the fluorescence was markedly higher in EL4 cells incubated with PS2 (PS2 PMA+) compared to any other evaluated formulation. This is clearly seen in Figure 3f. Furthermore, the same fluorescence intensity is observed for both PSs (Figure 3f) after pre-

incubation with NAC, ROS-scavenger[47] and treatment with PMA confirming that PS2 is able to selectively release its cargo into ROS-stimulated cancer cells.

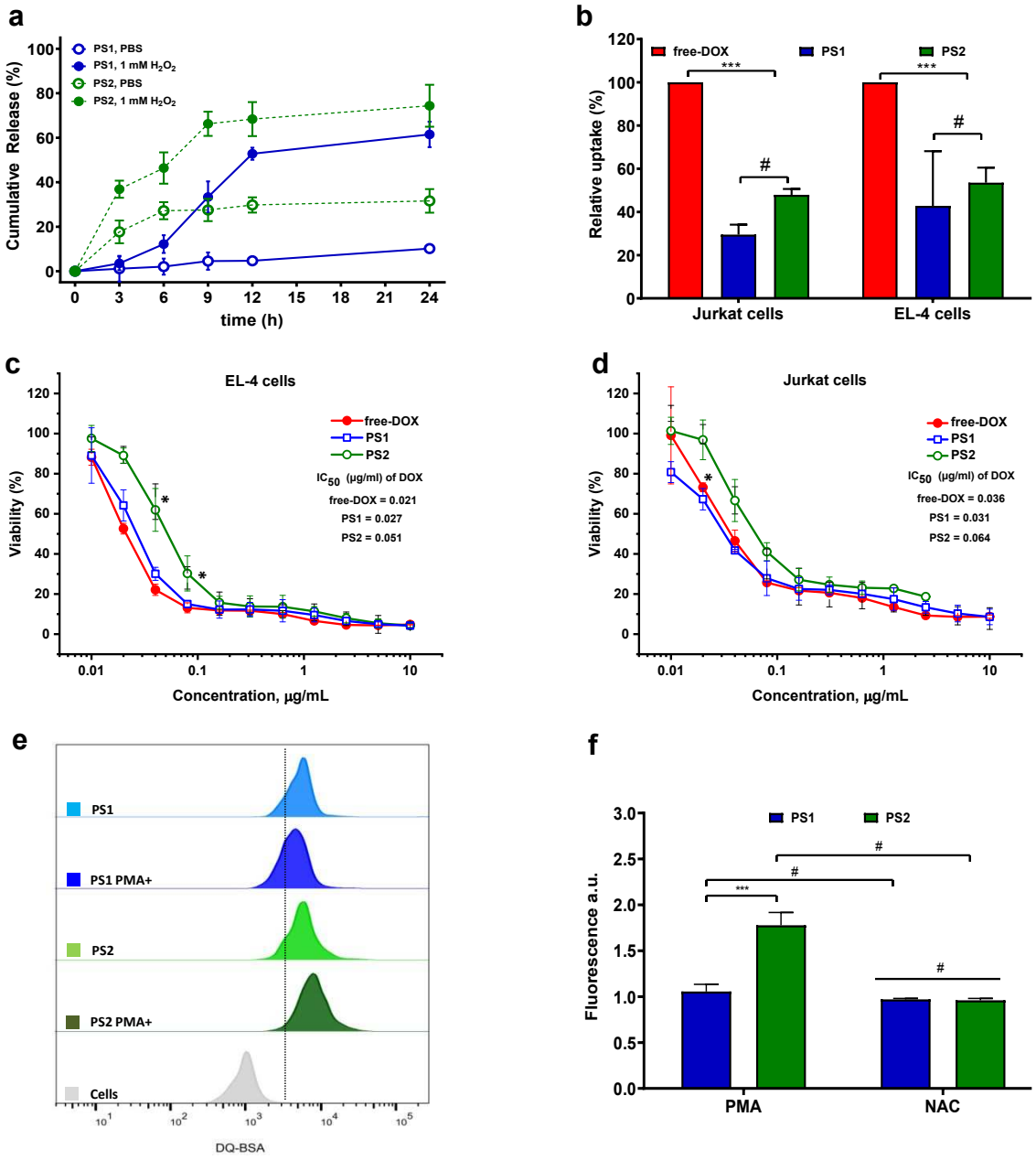

Figure 3 a) Doxorubicin cumulative release in PBS buffer pH 7.4 (open blue circles - PS1; open green circles - PS2) and in 1 mM H_2O_2 (solid blue circles - PS1; solid green circles - PS2) over 24 h (n=2). b) PSs and free DOX cellular uptake by Jurkat and EL4 tumor cell lines after 2 h

incubation time (n=4). Cell viability of EL4 (c) and (d) Jurkat cell lines after 72 h incubation time with different concentrations of free DOX (red circles) and DOX-loaded PS1 (blue squares) and DOX-loaded PS2 (green circles) (n=4). (e) Flow cytometry analysis of EL4 cells pre-incubated with PSs containing double-quenched bovine serum albumin (DQ-BSA) at the absence and presence of PMA (100 nM). (f) DQ-BSA release from PS1 and PS2 in the presence of PMA (100 nM; ROS-inducer) and in the presence of NAC (3mM; ROS-scavenger). Data are the ratio between cells treated and untreated with PMA or NAC (+PMA) (n=2). *$p < 0.05$; ***$p < 0.001$; # - non-significant.

In vivo assays

The biodistribution assays were performed using the fluorescent dye DBCO-Cyanine7 (Cy7, Figure S11) that can be detected in deep tissues.[48] The Cy7 was conjugated to the ROS-responsive BCs by copper-free click-chemistry reaction and the fluorescence *in vivo* was monitored after the administration of free Cy7 and Cy7-PSs. The *in vivo* imaging is provided in Figure 4a and the quantitative values in Figure 4b. The PSs accumulation is more noticeable in the liver, kidneys, spleen and tumor. The PSs accumulation is generally dependent on the administration route, size and chemistry (surface charge, hydrophilic shell, shell density). Nevertheless, higher accumulation in these organs is frequently reported.[48-51] The Free-Cy7 accumulated ~ 2-3 times less in the tumor compared with the PSs at longer incubation times, such as 3 to 7 days, which is most likely an effect of the long blood circulation promoted by the PSs (Figure 4a and c). The observed enhanced tumor accumulation with prolonged circulation times is favourable for the efficacy of the therapeutic treatment and is in agreement with the results obtained for other similar stealth nanomedicines.[43,49-54]

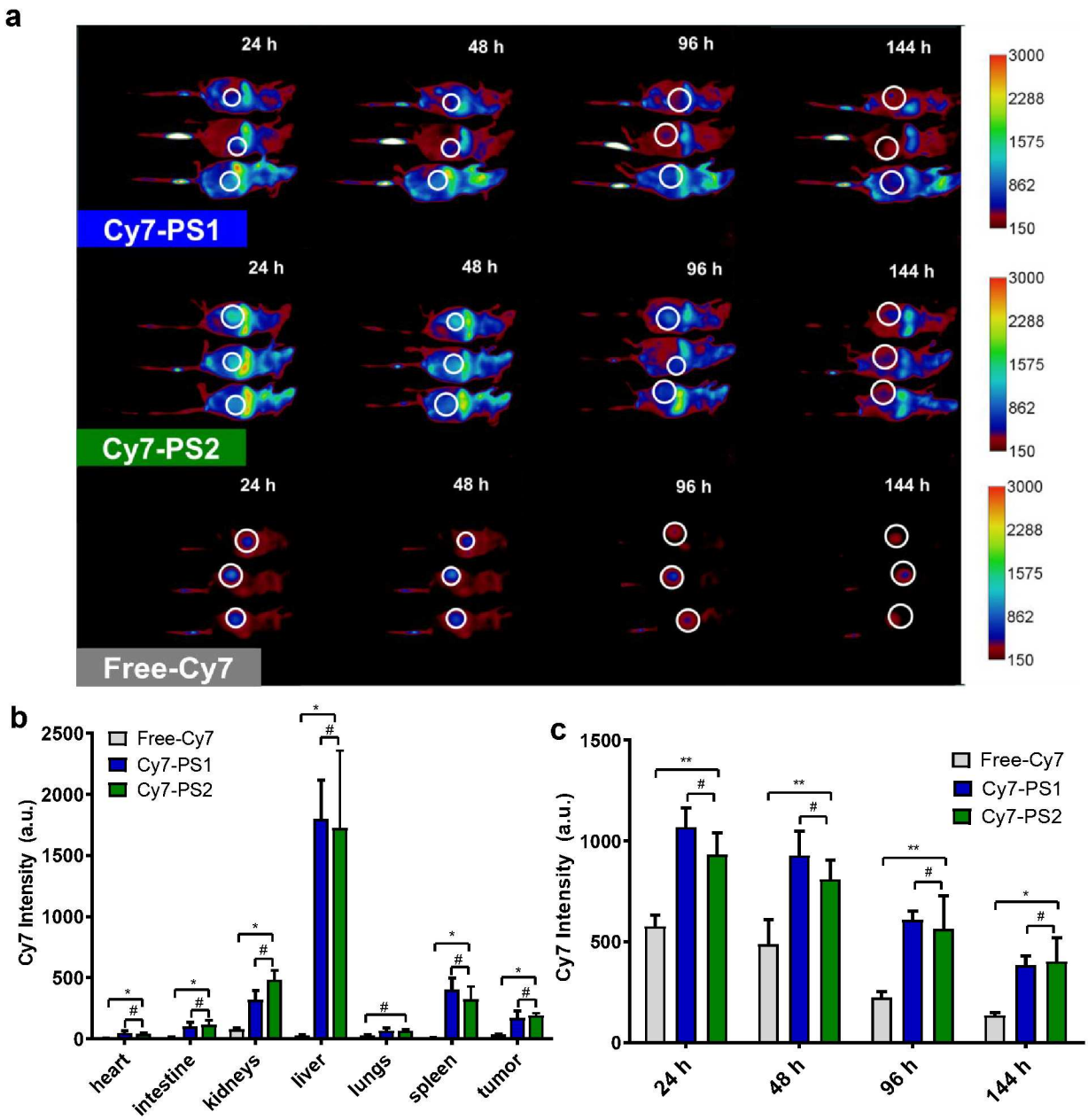

Figure 4 a) *In vivo* biodistribution analysis of Cy7-PSs and free fluorescent dye DBCO-Cy7 (Free-Cy7) over 144 h in mice bearing EL4 T lymphoma tumor. The mice were imaged in the right flank using Ex/Em = 750/830 nm filter pair to visualize the Cy7 dye (white circles refer to the tumor area). b) Cy7-PSs accumulation in different organs and in EL4 T lymphoma tumors after 7 days of PSs administration. (c) time-dependent accumulation of Cy7-PSs in EL4 T

lymphoma tumor compared to free Cy7 administration (* indicates statistical significance provided by one-way ANOVA * $p < 0.05$; ** $p < 0.01$; # non-significant - n= 3 mice/group).

The accumulation of Cy7-PS1 and Cy7-PS2 in the organs and in the tumor is similar as a consequence of the related features of the vesicles (size, shape and surface charge). Overall, these results demonstrated that the PSs circulate for reasonable long time *in vivo* suggesting that they are potentially able to promote the accumulation of loaded drugs into tumor sites thereby enhancing the effectiveness of chemotherapeutic treatments.

In line with this, it has been further evaluated the *in vivo* antitumor efficacy of the DOX-loaded polymersomes intravenously injected into the tail vein of mice bearing EL4 T cell lymphoma. DOX-loaded PS1 and PS2, PBS and free DOX were administered at dose of 5 mg DOX equivalent/kg after 7 days of tumor transplantation on days 0, 4 and 8 (named as days of treatment). The tumor growth and mouse survival were monitored and the results are provided in Figure 5. Enhanced suppression of tumor cell growth and extended survival time is observed when the animals were treated with PSs (Figure 5a-b). Additionally, side effects of the chemotherapeutic treatment are remarkably reduced when DOX was encapsulated into the polymersomes. This is evidenced by the balanced body weight (Figure 5c) and reduced DOX cardiotoxicity (one of its main shortcomings) as suggested by the reduction of serum creatine kinase levels monitored in mice blood (Figure 5d). Accordingly, the *in vivo* accumulation of PS1 and PS2 as well as *in vitro* cellular uptake (for EL4 cells) and cytotoxicity at concentrations higher than 0.1 $\mu g \cdot mL^{-1}$ are similar. Therefore, although PS2 demonstrates deprotection followed by self-immolative reaction releasing the cargo (DOX, DQ-BSA) to higher extent compared to

PS1, the efficacy in the treatment of lymphomas *in vivo* was similar for both evaluated ROS-responsive assemblies.

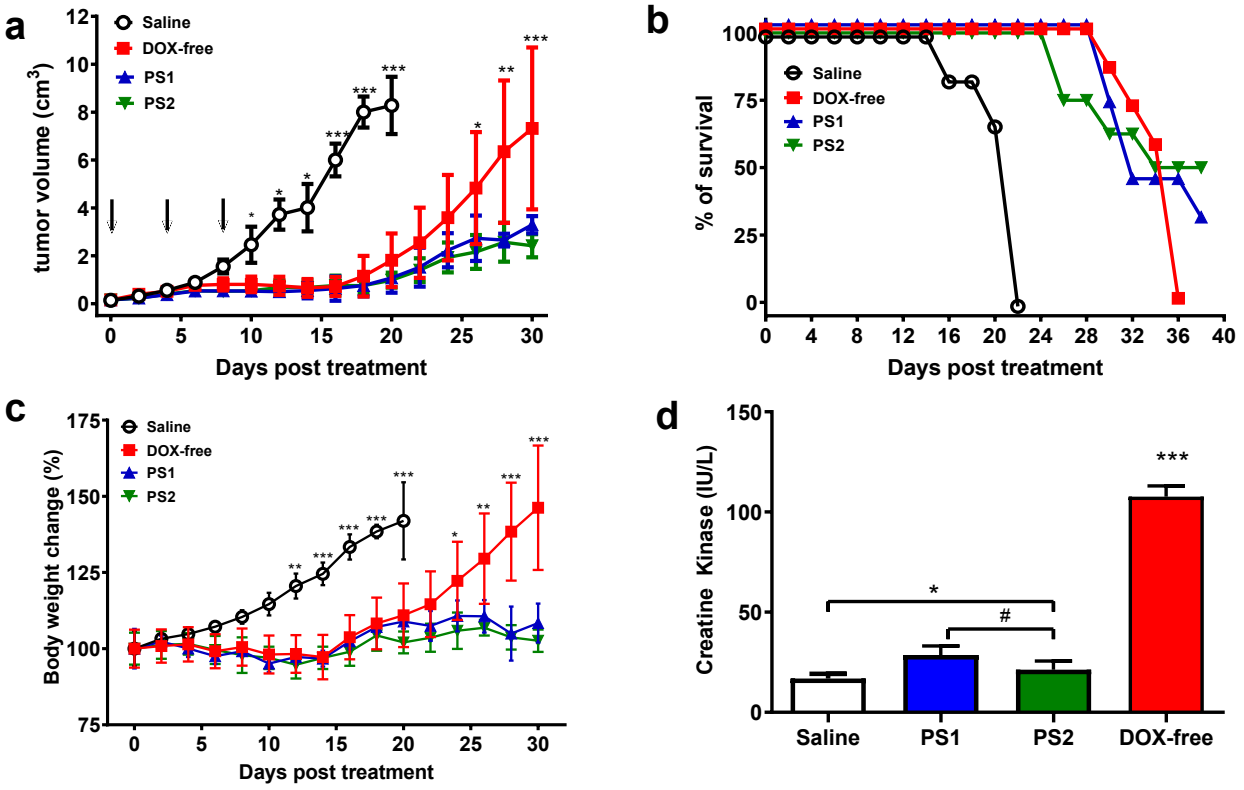

Figure 5 a) *In vivo* therapeutic effect of PSs, free DOX and saline in the growth of T cell lymphoma EL4 (black arrows indicate injections). b) Kaplan-Meier survival plot of mice after 3 × 5 mg DOX (equivalent)/kg administration and untreated control. c) Body weight changes during PSs and free DOX treatment. d) Serum creatine kinase levels in the blood after saline, free DOX, PS1 and PS2 administration in mice bearing EL4 T lymphoma. * $p < 0.05$; ** $p < 0.01$; *** $p < 0.001$; # non-significant. (Saline: n=6; free DOX: n=8; PS1: n=8; PS2: n=8).

CONCLUSIONS

We describe the successful development of ROS-responsive BCs to manufacture PSs with tunable site-specific release of the chemotherapeutic drug DOX. We demonstrated that BC and PSs chemistry influences the deprotection behavior, showing dependence on BC deprotection linkage and H_2O_2 conditions. The results from this pioneering work suggest that the ROS-responsive PSs produced exhibit the physicochemical and biological properties required for practical applications as nanomedicines with potential for tumor-targeting DOX delivery based on the ROS-triggered release mechanism *in vitro* and *in vivo*. Furthermore, the simplicity and effectiveness of the PSs approach and the ability to chemically modify the resulting particles ensure the application in various fields of research and for different disease treatments.

ASSOCIATED CONTENT

Supporting information

Synthetic route and molecular structures of PHPMA macroCTA, ROS-responsive monomers and BCs; SEC chromatograms of PHPMA macroCTA and of the BCs before and after deprotection; ^{1}H NMR spectra of PHPMA macroCTA and BCs; ^{1}H NMR spectra of the BCs during deprotection,; H_2O_2 scavenging ability test, Zimm-plot of the PSs before and after deprotection; TEM and cryo-TEM micrographs; cellular viability data. This material is available free of charge via the Internet at http://pubs.acs.org.

AUTHOR INFORMATION

Corresponding Authors

* (E.J.) E-mail: jager@imc.cas.cz;

Author Contributions

The manuscript was written through contributions of all authors. All authors have given approval to the final version of the manuscript.

Notes

The authors declare no competing financial interest.

ACKNOWLEDGMENTS

This work has been sponsored by the Czech Science Foundation (grant #17-09998S). A.J and V.S. acknowledges the Czech Ministry of Education, Youth and Sports (grant no. 8J18FR038). P.S acknowledges grant #LM2015064 ERIC and grant POLYMAT#LO1507. M.H Thanks to the Ministry of Health of the Czechia (grant#AZV16-30544A). F.C.G. and L.J.C.A. acknowledge FAPESP (grants 2017/00459-4 and 2017/11261-0). Electron microscopy was supported by TA CR (#TN01000008). The CAPI experiments were supported by Ministry of Education, Youth and Sports of the Czech Republic (Large RI Project LM2015062 Czech-BioImaging and SVV 260371/2019) and by European Regional Development Fund (Project No. CZ.02.1.01/0.0/0.0/16_013/0001775). The authors would like to thank Dr. Martijn Verdoes for his valuable comments and suggestions.

REFERENCES

(1) Siegel, R.; Naishadham, D.; Jemal, A. Cancer statistics, 2013. *CA Cancer J. Clin*. **2013**, *63,* 11-30.

(2) Rupp, T.; Zuckerman, D. Quality of Life, Overall Survival, and Costs of Cancer Drugs Approved Based on Surrogate Endpoints. *JAMA Intern*. *Med*. **2017**, *177*, 276-277.

(3) Maeda, H.; Khatami, M. Analyses of repeated failures in cancer therapy for solid tumors: poor tumor-selective drug delivery, low therapeutic efficacy and unsustainable costs. *Clin. Transl. Med*. **2018**, *7*, 1-20.

(4) Ellis, E.; Zhang, K.; Lin, Q.; Ye, E.; Poma, A.; Battaglia, G.; Loh, X.J.; Lee, T.-C. Biocompatible pH-responsive nanoparticles with a core-anchored multilayer shell of triblock copolymers for enhanced cancer therapy. *J*. *Mater*. *Chem*. *B*. **2017**, *5*, 4421-4425.

(5) Joseph, A.; Contini, C.; Cechin, D.; Nyberg, S.; Ruiz-Perez, L.; Gaitzsch, J.; Fullstone, G.; Tian, X.; Azizi, J.; Preston, J.; Volpe, G.; Battaglia, G. Chemotactic synthetic vesicles: Design and applications in blood-brain barrier crossing. *Sci*. *Adv*. **2017**, *3*, e1700362.

(6) Marget, M.; Bonduellea, C.; Lecommandoux, S. Multicompartmentalized polymeric systems: towards biomimetic cellular structure and function. *Chem*. *Soc*. *Rev*. **2013**, *42*, 512-529.

(7) Palivan, C.G.; Goers, R.; Najer, A.; Zhang, X.; Car, A.; Meier, W. Bioinspired polymer vesicles and membranes for biological and medical applications. *Chem*. *Soc*. *Rev*. **2016**, *45*, 377-411.

(8) Hu, X.; Zhang, Y.; Xie, Z.; Jing, X.; Belloti, A.; Gu, Z. Stimuli-Responsive Polymersomes for Biomedical Applications. *Biomacromolecules* **2017**, *18*, 649-673.

(9) Yao, P.; Zhang, Y.; Meng, H.; Sun, H.; Zhong, Z. Smart Polymersomes Dually Functionalized with cRGD and Fusogenic GALA Peptides Enable Specific and High-Efficiency Cytosolic Delivery of Apoptotic Proteins. *Biomacromolecules* **2019**, *20*, 184-191.

(10) Schatz, C.; Louguet, S.; Le Meins, J.F.; Lecommandoux, S. Polysaccharide-block-polypeptide copolymer vesicles: towards synthetic viral capsids. *Angew*. *Chem*. *Int*. *Ed*. *Engl*. **2009**, *48*, 2572-2575.

(11) Le Meins, J.F.; Sandre, O.; Lecommandoux, S. Recent trends in the tuning of polymersomes' membrane properties. *Eur. Phys. J. E* **2011**, *2*, 1-17.

(12) Rideau, E.; Dimova, R.; Schwille, P.; Wurm, F.R.; Landfester, K. Liposomes and polymersomes: a comparative review towards cell mimicking. *Chem. Soc. Rev.* **2018**, *47*, 8572-8610.

(13) Meng, F.; Zhong, Z.; Feijen, J.; Stimuli-Responsive Polymersomes for Programmed Drug Delivery. *Biomacromolecules* **2009**, *10*, 197-209.

(14) Peters, R.J.R.w.; Marguet, M.; Marais, S.; Fraaije, M.W.; Van Hest, J.C.M., Lecommandoux, S. Cascade reactions in multicompartmentalized polymersomes. *Angew. Chem. Int. Ed. Engl.* **2014**, *53*, 146-150.

(15) Chen, W.; Meng, F.; Cheng, R.; Zhong, Z. pH-Sensitive degradable polymersomes for triggered release of anticancer drugs: A comparative study with micelles. *J. Control. Release* **2010**, *142*, 40-46.

(16) Lee, J.S.; Feijen, J. Polymersomes for drug delivery: Design, formation and characterization. *J. Control. Release* **2012**, *161*, 473-483.

(17) Oliveira, H.; Peres-Andres, E.; Thevenot, J.; Sandre, O.; Berra, E.; Lecommandoux, S. Magnetic field triggered drug release from polymersomes for cancer therapeutics. *J. Control. Release* **2013**, *169*, 165-170.

(18) Che, H.; Hest, J.C.M. Adaptive Polymersome Nanoreactors. *ChemNanoMat* **2019**, *5*, 1092-1109.

(19) Deng, Z.; Hu, J.; Liu, S. Reactive Oxygen, Nitrogen, and Sulfur Species (RONSS)-Responsive Polymersomes for Triggered Drug Release. *Macromol. Rapid Commun.* **2017**, *38*, 1600685.

(20) Tanner, P.; Balasubramanian, V.; Palivan, C.G. Aiding Nature's Organelles: Artificial Peroxisomes Play Their Role. *Nano Lett*. **2013**, *13*, 2875-2883.

(21) Richard, P.U.; Craciun, I.; Gaitzsch, J.; Weiner, L.; Palivan, C.G. Delivery of ROS Generating Anthraquinones Using Reduction-Responsive Peptide-Based Nanoparticles. *Helv. Chim. Acta* **2018**, *101*, e1800064.

(22) Kim, K.T.; Cornelissen, J. J. L. M.; Nolte, R.J.M.; van Hest, J. C. M. A Polymersome Nanoreactor with Controllable Permeability Induced by Stimuli-Responsive Block Copolymers. *Adv. Mater*. **2009**, *21*, 2787-2791.

(23) Liou, G.Y.; Storz, P. Reactive oxygen species in cancer. *Free Radic. Res*. **2010**, *44*, 479-496.

(24) Minelli, A.; Bellezza, I.; Conte, C.; Culig, Z. Oxidative stress-related aging: A role for prostate cancer? *Biochim Biophys Acta*. **2009**, *1795*, 83-91.

(25) Hancock, J.T.; Desikan, R.; Neill, S.J. Role of reactive oxygen species in cell signalling pathways. *Biochem. Soc. Trans*. **2001**, *29*, 345-350.

(26) D'Autréaux, B.; Toledano, M.B.; ROS as signalling molecules: mechanisms that generate specificity in ROS homeostasis. *Nat. Rev. Mol. Cell Biol*. **2007**, *8*, 813-824.

(27) Ye, H.; Zhou, Y.; Liu, X.; Chen, Y.; Duan, s.; Zhu, R.; Liu, Y.; Yin, L. Recent Advances on Reactive Oxygen Species-Responsive Delivery and Diagnosis System. *Biomacromolecules* **2019**, *20*, 2441-2463.

(28) Albuquerque, L.J.C.; Sincari, V.; Jäger, A.; Konefał, R.; Pánek, J.; Černoch, P.; Pavlova, E.; Štěpánek, P.; Giacomelli, F.C.; Jäger, E. Microfluidic-assisted engineering of quasi-monodisperse pH-responsive polymersomes toward advanced platforms for the intracellular delivery of hydrophilic therapeutics. *Langmuir* **2019**, *35*, 8363-8372.

(29) Zhao, W. Lighting up H_2O_2: the molecule that is a "necessary evil" in the cell. *Angew Chem Int Ed Engl*. **2009**, *48*, 3022-3024.

(30) Lin, V.S.; Dickinson, B.C.; Chang, C.J. Boronate-based fluorescent probes: imaging hydrogen peroxide in living systems. *Methods Enzymol*. **2013**, *526*, 19-43.

(31) Lux, C. D.G.; Joshi-Barr, S.; Nguyen, T.; Mahmoud, E.; Schopf, E.; Fomina, N.; Almutairi, A. Biocompatible polymeric nanoparticles degrade and release cargo in response to biologically relevant levels of hydrogen peroxide. *J*. *Am*. *Chem*. *Soc*. **2012**, *134*, 15758-15764.

(32) Stubelius, A, Lee, S.; Almutairi, A. The Chemistry of Boronic Acids in Nanomaterials for Drug Delivery. *Acc*. *Chem*. *Res*. **2019**, *52*, 3108-3119.

(33) Wang, J. Wang, X. Zhang, S. Yu, D. Wen, Q. Hu, Y. Ye, H. H. Bomba, X. Hu, Z. Liu, G. Dotti, Z. Gu, In situ formed reactive oxygen species-responsive scaffold with gemcitabine and checkpoint inhibitor for combination therapy. *Sci*. *Transl*. *Med*. **2018**, *10*, eaan3682.

(34) Jäger, E.; Höcherl, A.; Janoušková, O.; Jäger, A.; Hrubý, M.; Konefał, R.; Netopilik, M.; Pánek, J.; Šlouf, M.; Ulbrich, K.; Štěpánek, P. Fluorescent boronate-based polymer nanoparticles with reactive oxygen species (ROS)-triggered cargo release for drug-delivery applications. *Nanoscale* **2016**, *8*, 6958.

(35) Liang, X.; Duan, J.; Li, X.; Zhu, X.; Chen, Y.; Wang, X.; Sun, H.; Kong, D, Li, C.; Yang, J. Improved vaccine-induced immune responses via a ROS-triggered nanoparticle-based antigen delivery system. *Nanoscale*, **2018**, *10*, 9489-9503.

(36) Lebleu, C.; Rodrigues, L.; Guigner, J.-M.; Brulet, A.; Garanger, E.; Lecommandoux, S. Self-Assembly of PEG-*b*-PTMC Copolymers: Micelles and Polymersomes Size Control. *Langmuir* **2019**, *35*, 13364-13374.

(37) Castro, C.E. de.; Mattei, B.; Riske, C.A.; Jäger, E.; Jäger, A.; Štěpánek, P, Giacomelli, F.C. Understanding the Structural Parameters of Biocompatible Nanoparticles Dictating Protein Fouling. *Langmuir* **2014**, *30*, 9770-9779.

(38) Zhang, Q.; Zhang, F.; Chen, Y.; Dou, Y.; Tao, H.; Zhang, D.; Wang, R.; Li, X.; Zhang, J. Structure-Property Correlations of Reactive Oxygen Species-Responsive and Hydrogen Peroxide-Eliminating Materials with Anti-Oxidant and Anti-Inflammatory Activities. *Chem*. *Mater*. **2017**, *29*, 8221-8238.

(39) Bur, H.; Haapasaari, K-M.; Turpeenniemi-Hujanen, T.; Kuittinen, O.; Auvinen, O.; Marin, K.; Koivunen, P.; Sormunen, R.; Soini, Y.; Karihtala, P. Oxidative stress markers and mitochondrial antioxidant enzyme expression are increased in aggressive Hodgkin lymphomas. *Histopathology* **2014**, *65*, 319-327.

(40) Klaunig, J.E.; Xu, Y.; Isenberg, J.S.; Bachowski, S.; Kolaja, K.L.; Jiang, J.; Stevenson, D.E.; Walborg Jr, E.F. *Environ*. *Health Perspect*. **1998**, *106*, 289-295.

(41) Liu, Y.; Fang, J.; Kim, Y.-J.; Wong, M.K.; Wang, P. Codelivery of Doxorubicin and Paclitaxel by Cross-Linked Multilamellar Liposome Enables Synergistic Antitumor Activity. *Mol*. *Pharmaceutics* **2014**, *11*, 1651-1661.

(42) Strozyk, M.S.; Carregal-Romero, S.; Henriksen-Lacey, M.; Brust, M.; Liz-Marzan, L.M. Biocompatible, Multiresponsive Nanogel Composites for Codelivery of Antiangiogenic and Chemotherapeutic Agents. *Chem*. *Mater*. **2017**, *29*, 2303-2313.

(43) Cui, C.; Xue, Y.-N.; Wu, M.; Zhang, Y.; Yu, P.; Liu, L.; Zhuo, R.-X.; Huang, W. Cellular uptake, intracellular trafficking, and antitumor efficacy of doxorubicin-loaded reduction-sensitive micelles. *Biomaterials* **2013**, *34*, 3858-3869.

(44) Hu, X.; Liu, S.; Huang, X.; Chen, X.; Jing, X. Biodegradable Block Copolymer-Doxorubicin Conjugates via Different Linkages: Preparation, Characterization, and In Vitro Evaluation. *Biomacromolecules* **2010**, *11*, 2094-2102.

(45) Bull, C.; Boltje, T.J.; Van Dinther, E.A.W.; Peter, T.; De Graaf, A.M.A.; Lausen, J.H.W.; Kreutz, M.; Figdor, C.G.; Den Brok, M.H.; Adema, G.J. Targeted Delivery of a Sialic Acid-Blocking Glycomimetic to Cancer Cells Inhibits Metastatic Spread. *ACS Nano* **2015**, *9*, 733-745.

(46) Nunes-Hasler, P.; Maschalidi, S.; Lippens, C.; Castelbou, C.; Bouvet, S.; Guido, D.; Bermont, F.; Bassoy, E.Y.; Page, N.; Merkler, D.; Hugues, S.; Martinvalet, D.; Manoury, B.; Demaurex, N. *Nat*. *Commun*. **2017**, *8*, 1852.

(47) Halasi, M.; Wang, M.; Chavan, T.S.; Gaponenko, V.; Hay, N.; Gartel, A.L. ROS inhibitor *N*-acetyl-L-cysteine antagonizes the activity of proteasome inhibitors. *Biochem*. *J*. **2013**, *454*, 201-208.

(48) Yang, K.; Zhang, S.; Zhang, G.; Sun, X.; Lee, S.T.; Liu, Z. Graphene in Mice: Ultrahigh In Vivo Tumor Uptake and Efficient Photothermal Therapy. *Nano Lett*. **2010**, *10*, 3318-3323.

(49) Photos, P.J.; Bacakova, L.; Discher, B.; Bates, F.S.; Discher, D.E. Polymer vesicles in vivo: correlations with PEG molecular weight. *J*. *Control*. *Release* **2003**, *90*, 323-334.

(50) Chiang, Y.-T.; Cheng, Y.-T.; Lu, C.-Y.; Yen, Y.-W.; Yu, L.-Y.; Lyu, S.-Y.; Yang, C.-Y.; Lo, C.-L. Polymer-Liposome Complexes with a Functional Hydrogen-Bond Cross-Linker for Preventing Protein Adsorption and Improving Tumor Accumulation. *Chem*. *Mater*. **2013**, *25*, 4364-4372.

(51) Jeannot, V.; Gauche, C.; Mazzaferro, S.; Couvet, M.; Vanwonterghen, L.; Henry, M.; Dider, C.; Vollaire, J.; Josserand, V.; Col, J.-L.; Schatz, C.; Leccommandoux, S.; Hurbin, A. Anti-

tumor efficacy of hyaluronan-based nanoparticles for the co-delivery of drugs in lung cancer. *J. Control. Release* **2018**, *275*, 117-128.

(52) Qiu, M.; Zhang, Z.; Wei, Y.; Sun, H.; Meng, F.; Deng, C; Zhong, Z. Small-Sized and Robust Chimaeric Lipopepsomes: A Simple and Functional Platform with High Protein Loading for Targeted Intracellular Delivery of Protein Toxin in Vivo. *Chem. Mater.* **2018**, *30*, 6831-6838.

(53) Kwon, G.S.; Kataoka, K. Block copolymer micelles as long-circulating drug vehicles. *Adv. Drug Deliv. Rev.* **1995**, *16*, 295-309.

(54) Lee, J.S.; Ankone, M.; Peiters, E.; Schiffelers, R.M.; Hennink, W.W.; Feijen, J. Circulation kinetics and biodistribution of dual-labeled polymersomes with modulated surface charge in tumor-bearing mice: Comparison with stealth liposomes. *J. Control. Release* **2011**, *155*, 282-288.

Graphical Abstract

(For Table of Contents Use Only)

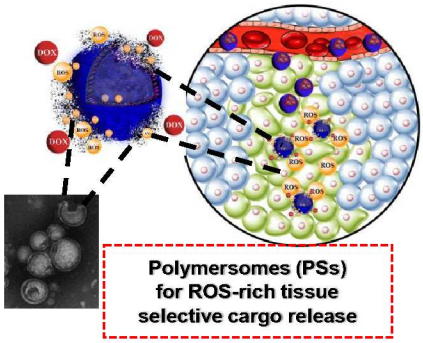

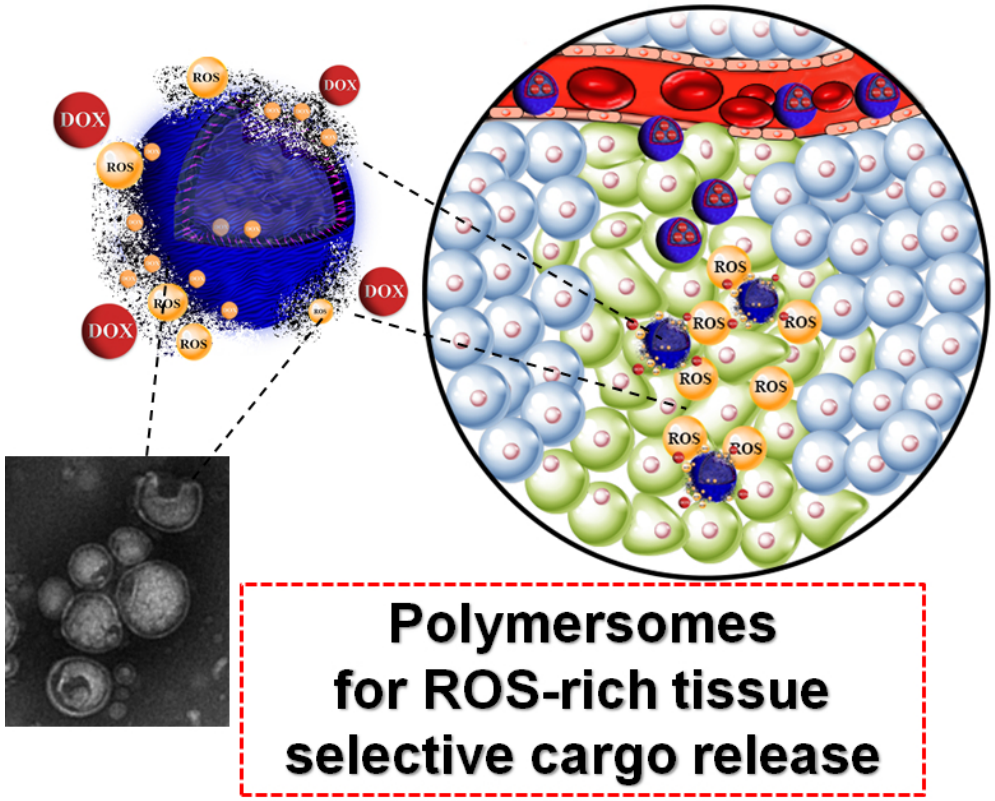

66x54mm (300 x 300 DPI)